INTERNATIONAL JOURNAL FOR NUMERICAL METHODS IN FLUIDS
Int. J. Numer. Meth. Fluids 2004; **46**:289–313 (DOI: 10.1002/fld.759)

Grid-free surface vorticity method applied to flow induced vibration of flexible cylinders

K. Lam[1,*,†], G. D. Jiang[2], Y. Liu[1] and R. M. C. So[1]

[1]*Department of Mechanical Engineering, The Hong Kong Polytechnic University, Hong Kong*
[2]*Xi'an Jiaotong University, Xi'an, P. R. China*

SUMMARY

In order to study cross flow induced vibration of heat exchanger tube bundles, a new fluid–structure interaction model based on surface vorticity method is proposed. With this model, the vibration of a flexible cylinder is simulated at $Re = 2.67 \times 10^4$, the computational results of the cylinder response, the fluid force, the vibration frequency, and the vorticity map are presented. The numerical results reproduce the amplitude-limiting and non-linear (lock-in) characteristics of flow-induced vibration. The maximum vibration amplitude as well as its corresponding lock-in frequency is in good agreement with experimental results. The amplitude of vibration can be as high as $0.88D$ for the case investigated. As vibration amplitude increases, the amplitude of the lift force also increases. With enhancement of vibration amplitude, the vortex pattern in the near wake changes significantly. This fluid–structure interaction model is further applied to simulate flow-induced vibration of two tandem cylinders and two side-by-side cylinders at similar Reynolds number. Promising and reasonable results and predictions are obtained. It is hopeful that with this relatively simple and computer time saving method, flow induced vibration of a large number of flexible tube bundles can be successfully simulated. Copyright © 2004 John Wiley & Sons, Ltd.

KEY WORDS: flow induced vibration; fluid–structure interaction; surface vorticity method

1. INTRODUCTION

Flow induced vibration (FIV) is one of the major concerns in the design of modern heat exchangers. Heat exchanger tube failures due to FIV are costly because they could result in plant shutdown for very expensive repairs. The flow around heat exchanger tube bundles is very complex, especially when the tubes are flexible. The motions of the tubes and their effects on the surrounding flow increase the complexity of the problem.

*Correspondence to: K. Lam, Department of Mechanical Engineering, The Hong Kong Polytechnic University, Hung Hom, Kowloon, Hong Kong.
†E-mail: mmklam@polyu.edu.hk

Contract/grant sponsor: Research Grants Council of the Hong Kong Special Administration Region, China; contract/grant number: Poly U5163/01E

Published online 29 July 2004

Received 5 May 2003
Revised 15 November 2003

Over the past 30 years, FIV of heat exchanger tube bundles has received a great deal of attention from researchers. Excellent reviews of flow induced vibration in heat exchanger tube bundles have been given by Weaver and Fitzpatrick [1]. Numerous experimental investigations have been conducted to study the mechanism of FIV in different configurations of tube bundles. Ziada and Oengoren [2], Zdravkovich [3], Polak and Weaver [4], Austermann [5], Romberg and Popp [6], and Chen and Srikantiah [7] have made various contributions on the experimental investigations of FIV in in-line and staggered geometry of tube bundles in heat exchanger. Some instability models [8] and design criteria [9] have been developed for predicting the instability of tube bundles in various configurations based on experimental results.

Compared to experimental studies, there have been relatively few numerical investigations in flow induced vibration problems. Generally computational fluid dynamics (CFD) methods can be divided into two main categories, namely grid-based methods and grid-free methods. Grid-based CFD methods, such as finite difference method (FDM), Finite element method (FEM), and the newly developed spectral element method (SEM), have been successfully used to simulate flow induced vibration of single flexible cylinder at low Reynolds numbers [10–12]. In addition, there are some encouraging results from simulation of flow induced vibration of multi-cylinders using grid-based method. Ichioka *et al.* [13] applied FDM to simulate the vibration of two cylinders and a cylinder row in a cross flow at Reynolds number, $Re = 1000$ and 6000–10 000. Kassera and Strohmeier [14] computed the flow induced vibration of six different tube bundles using FDM at $Re = 200\,000$, and Schroder and Gelbe [15] did the simulation of tube bundle at $Re = 140\,000$. Liu *et al.* [16] computed the flow induced vibration of two side-by-side circular cylinders using FEM at $Re = 200$, while Mittal and Kumar [17] calculated flow induced oscillation of a pair of cylinders in tandem and in staggered arrangement using FEM at $Re = 160$. Besides consideration of computational accuracy and costs, grid-based methods are still at their infancy for the simulation of flexible tube arrays at practical *Re* range due to the large number of meshes and mesh redistribution when the tubes vibrate.

Grid-free methods, classified as discrete vortex method and surface vorticity method (SVM), plays an important role in the study of flow around bluff bodies since they concentrate on the vorticity field and directly capture the physical nature of the flow around bluff bodies. They are very suitable for flow induced vibration problems, because the bodies can be allowed to move freely over a large distance without the limitation of the grid. However, compared with grid-based method, published work on flow induced vibration investigations using grid-free CFD method is scarce. Slaouti and Stansby [18] published their results of flow induced vibration of a flexible cylinder using discrete vortex method incorporated with vortex-in-cell (VIC) technology, while Zhou *et al.* [19] systematically simulated the flow induced vibration of an elastic circular cylinder at $Re = 200$ using the same technique. Although VIC provides substantial savings to the computational time, it makes the method grid-dependent. Since body-fitted coordinates are required, the extension of the VIC method to similar problems with multi-cylinder vibration would be rather difficult, if not impossible.

The SVM with moving separation points has been successfully applied to calculate flow around rigid cylinders in the high sub-critical *Re* range [20, 21]. Although the two-dimensional (2-D) computational model does not completely replicate the 3-D near wake of the flow behind the cylinder, it is able to simulate most of the prominent characteristics (such as fluid forces and shedding frequency) of the flow around cylinders. Furthermore, even for the

meshed method, 3-D numerical modelling related to the complex wake flow is still mostly being confined to low Reynolds number conditions. In order to correctly predict the structure response of the flow induced vibration problem, more emphasis has been put on how to correctly reproduce the vortex shedding frequency and the amplitude of the unsteady forces than to replicate the 3-D turbulent wake flow. However, SVM has not been used to solve flow induced vibration problems because of the lack of a suitable fluid–cylinder interaction model. Therefore, it is very important to develop an appropriate fluid–structure interaction model based on SVM. This model should reflect the coupling between vorticity and the vibrating body, and yet can take advantage of the grid-free nature of SVM to allow its extension to multi-cylinder vibration problems.

Therefore in the present paper the flow around a single cylinder in free-stream condition is examined first in order to verify the shedding frequency and unsteady force amplitude. The primary objective of the present study is to model the cross flow induced vibration of flexible cylinders at high sub-critical *Re* based on SVM. A new fluid–structure coupling model accounting for the interaction of vorticity field and flexible cylinders is proposed. This model is then applied to calculate the vibration of a freely suspended cylinder, and its result is compared with experimental and other numerical data. Finally, as an initial attempt, the flow induced vibration of two independently moving tandem cylinders and two independently moving side-by-side cylinders is simulated.

2. NUMERICAL FORMULATION

In the simulation of fluid–structure interaction problems, it is necessary to calculate first the flow dynamics, then the structural dynamics and finally the fluid–structure interaction. Therefore, in the following, the SVM for flow calculation and the 2-D structural dynamic model are introduced first, and then the newly developed fluid–structure interaction model and the coupling between the vorticity field and the flexible cylinders are discussed.

2.1. *Surface vorticity method* (*SVM*)

The fluid dynamics is governed by the Navier–Stokes equations. For 2-D incompressible flow, the governing equations can be converted to the following vorticity transport equation:

$$\frac{\partial \omega}{\partial t} + \vec{V} \bullet \nabla \omega = \nu \nabla^2 \omega \tag{1}$$

Therefore, flow development can be regarded as vorticity generation (shedding), $\partial\omega/\partial t$, vorticity convection, $\vec{V} \bullet \nabla\omega$, and the diffusion of vorticity, $\nu\nabla^2\omega$. Here ω is the vorticity, $\vec{V}$ the velocity, t is the time, and ν is the fluid kinematic viscosity.

In the SVM, the continuous vorticity distribution in the boundary layer of a bluff body is represented by a number of vortex elements, which are called surface vortices, to satisfy the zero normal velocity and zero slip condition. The strength of the surface vortex elements is calculated using Martensen's potential flow method taking into account the additional coupling effects of free vortices [22]. Consequently, the strength of the mth surface vortex element can

be represented by

$$\sum_{n=1}^{M} \gamma(s_n)K(s_n,s_m)\Delta s_n = -U\left[\frac{\mathrm{d}x_m}{\mathrm{d}s_m}\cos\alpha + \frac{\mathrm{d}y_m}{\mathrm{d}s_m}\sin\alpha\right] + \sum_{i=1}^{I}\Delta\Gamma_i L(i,m) \tag{2}$$

where $\gamma(s_n)$ is the nth surface vortex strength, $K(s_n,s_m)$ is the coupling coefficient of the nth surface vortex to the mth surface vortex, Δs_n is the length of the nth surface vortex element, U is the mainstream velocity, α is the angle between the x-direction and the mainstream direction, $\mathrm{d}x_m/\mathrm{d}s_m$ and $\mathrm{d}y_m/\mathrm{d}s_m$ are the projection factors of the x-direction and y-direction to the surface tangent direction, respectively, $\Delta\Gamma_i$ is the vorticity of the ith free vortex, $L(i,m)$ is the coupling coefficient of the ith free vortex to the mth surface vortex element, M is the total number of surface vortex, and I is the total number of free vortex.

At each time step the separation points on the surface are determined by a velocity direction scheme (VDS). Then the surface vortices behind the separation point are shed from the surface at a tiny distance normal to the surface and become free vortices (Rankine vortices). The free vortices move in the flow field under the influence of the convection velocity, the surface vortices and other free vortices, and viscous diffusion of the free vortices. The convection influence for the free vortices is considered by the Biot–Savart induction theorem [22]. The viscous diffusion of free vortices is evaluated by the diffusion velocity method proposed by Ogami and Akamatsu [23]. The surface vortices are also affected by the moving free vortices, which account for the additional term in Martensen's potential flow equation. Consequently, the vorticity distribution in the flow field can be determined. Furthermore the velocity field can be calculated from the vorticity distribution.

2.1.1. Velocity direction scheme. Separation point determination is very important when SVM is used to simulate flow around bluff bodies. Lewis [22] used the fixed separation point shedding to simulate flow separation around a cylinder. For flow around multi-cylinders, due to the interference among cylinders, the separation positions are different for each cylinder at different cylinder configuration. When the cylinders vibrate, the separation points also fluctuate along the surface. Therefore, a suitable method should be proposed to handle the change in the locations of the separation points.

It is argued that the separation of shear layer from the wall is the consequence of the influence of the historical development of the ever-changing free shear layers behind the cylinders. Hence a velocity direction scheme is adopted to locate the separation points. Figure 1 is the sketch of velocity vectors near the body surface in two different situations. The velocity vectors at two small distances, one shedding distance ε and the other at double the shedding distance 2ε, near the surface are calculated. If the velocity vector at 2ε is converging with that at ε, such as shown in Figure 1(a), the surface vortex at that position will remain as bounded vortices and boundary separation will not occur. On the other hand, if the velocity vector at 2ε is diverging with that at ε, such as shown in Figure 1(b), the surface vortex will become a free vortex. A free shear layer will then develop and boundary layer separation will take place. Hence, at each time step, the position of the separation point may change according to the relative direction of the two velocity vectors. This scheme is therefore called the velocity direction scheme for the determination of flow separation.

For the sub-critical Reynolds number examined in the present paper, the experimental result of the separation points for a single cylinder is found to be around $78^\circ \pm 3^\circ$ starting from the front stagnant point [24]. Through the numerical experiment, it is found that with a shedding

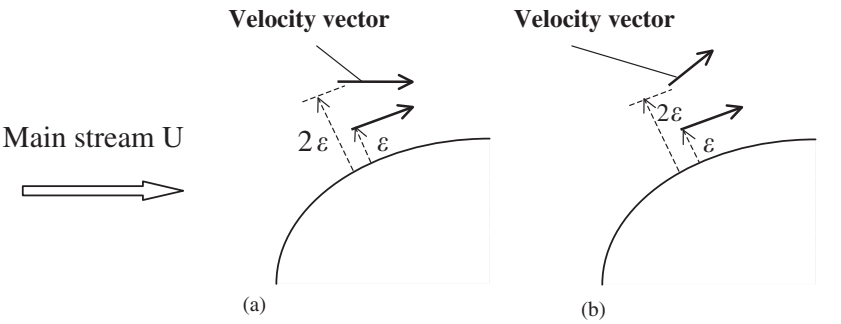

Figure 1. Sketch of velocity direction scheme (VDS) for separation point determination. (a) Velocity vectors converging before separation; (b) after separation.

distance ε equals $0.01D$ (D is the diameter of the cylinder) and the vortex element number equals 30, the separation point calculated by VDS is about 78°. Hence in the present paper, the above shedding distance and vortex element number parameters are used throughout the simulation.

2.1.2. Calculation of the force coefficients. The pressure distribution around the cylinder is calculated using the energy equation and by accounting for the dynamic pressure loss across the free layer used by Lewis [25], that is, the dimensionless static pressure coefficients are as follows:

$$C_p = C_{p0} - (u_s/U)^2 \quad \text{upstream of the separation point} \tag{3}$$

$$C_p = C_{p0} - (u_s/U)^2 - (u_{sp}/U)^2 \quad \text{downstream of the separation point} \tag{4}$$

where C_p is the dimensionless pressure coefficient, C_{p0} is the dimensionless stagnation point pressure coefficient, u_s is the surface vorticity velocity, and u_{sp} is the surface velocity at the separation point. At sub-critical Re, the effect of skin friction on the mean drag of a bluff body is negligibly small. Therefore, the lift and drag coefficient can be obtained by integrating the pressure coefficients around the bluff body alone, i.e.

$$C_D = \frac{1}{2}\int_0^{2\pi} C_p \cos\theta \, d\theta \tag{5}$$

$$C_L = \frac{-1}{2}\int_0^{2\pi} C_p \sin\theta \, d\theta \tag{6}$$

where θ is the circumferential location of C_p.

2.2. Structural dynamics

Since the flow is 2-D, unsteady forces act on the cylinder along the x- and y-direction. If the cylinder is further assumed to have a two-degree-of-freedom motion only (bending motion in the x- and y-direction), a 2-D spring–damper–mass model can represent it, and the motion of the cylinder can be described by the following 2-D dynamic equations written in

dimensionless form as

$$\ddot{X} + \frac{4\pi\zeta_S}{U_r}\dot{X} + \left(\frac{2\pi}{U_r}\right)^2 X = \frac{C_D}{2M} \tag{7}$$

$$\ddot{Y} + \frac{4\pi\zeta_S}{U_r}\dot{Y} + \left(\frac{2\pi}{U_r}\right)^2 Y = \frac{C_L}{2M} \tag{8}$$

where $X = x/D$, $Y = y/D$, x and y are the instantaneous positions of the cylinder in the x- and y-direction, respectively, D is the diameter of the cylinder, $\zeta_S = c/(2\sqrt{km})$ is the dimensionless structural damping coefficient, c is the damping coefficient, k is the equivalent stiffness, m is the cylinder mass per unit length, $U_r = U/(f_N D)$ is the reduced velocity, f_N is the natural frequency of the rigid cylinder, $M = m/(\rho D^2)$ is the mass ratio, and ρ is the fluid density. These dynamic equations are solved using the Runge–Kutta method. Once the equations are solved, the velocity of the cylinder and its displacements can be determined.

2.3. Fluid–structure interaction model

The flow chart of the vortex–cylinder interaction simulation is shown in Figure 2. The reference coordinates is fixed with the flow field and all the cylinders are vibrating relative to the reference coordinate. At each time step, the vorticity field is determined by the SVM at first. Then the forces acting on the cylinders are calculated using Equations (5) and (6), and then the displacement and velocity of the cylinders are computed by the Runge–Kutta method using Equations (7) and (8). At last, the cylinders and the vorticity are moved according to the calculated cylinder displacements, while the strength of the surface vortices on each cylinder is changed under the influence of the cylinder velocity. The modified vorticity distribution caused by the vibration of the cylinders will affect the fluid forces in the next time step. In such a process, the fluid forces, the cylinder vibrations, and the vorticity field are evaluated in an iterative way so that the interactions between fluid and cylinder are simulated.

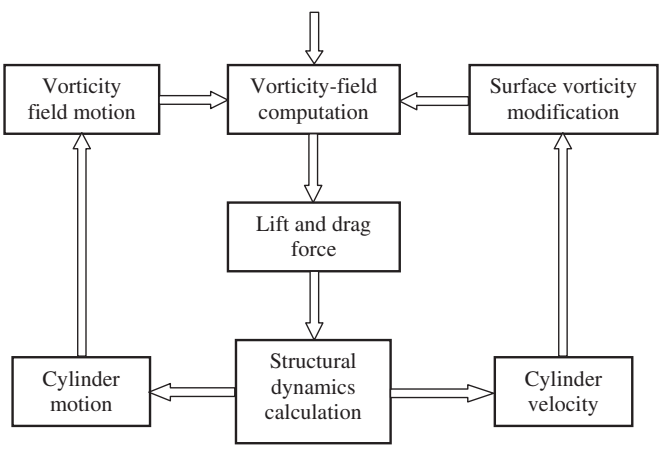

Figure 2. Flow chart of fluid–structure coupling simulating based on SVM.

For a successful fluid–structure interaction model, the most important points are how the flow field acts on the cylinder and how the cylinder vibrations influence the flow field (in this case it is how the structural vibrations influence the vorticity field). Solution of the former has been detailed in Section 2.2, while the latter is discussed in the next section.

2.3.1. Effect of cylinder movement on the vorticity field. The cylinders are located in a vorticity field with an infinite outside boundary. When the flexible cylinder moves under the action of fluid forces, the vortices contained within the fluid medium also move together with the continuum. The number and the strength of the vortices will remain unchanged. The farther away the vortices to the cylinder, the smaller the distance the vortices move. Hence a simplified model is proposed. When the cylinder is moved, the displacement of free vortices around it is considered to be inversely proportional to the nth power of the vortex-to-cylinder distance. Therefore, if they are only one moving cylinder, the displacement of a vortex is determined by the displacement of the cylinder and the vortex-to-cylinder distance, if they are more than one moving cylinders, the displacement of a vortex is the sum of that caused by each moving cylinder. That is,

$$X_{Vj} = \sum_i X_{Ti} \frac{1}{d_{ij}^n} \tag{9}$$

$$Y_{Vj} = \sum_i Y_{Ti} \frac{1}{d_{ij}^n} \tag{10}$$

where X_{Vj} and Y_{Vj} are the displacements of the jth vortex, X_{Ti} and Y_{Ti} are the displacements of the ith cylinder, d_{ij} is the distance between the jth vortex and the ith cylinder, and n is the power. In the present study, n is chosen to be unity.

2.3.2. Effect of structural motion on surface vorticity. For rigid cylinders in a uniform stream, the strength of the surface vortices is determined by Equation (2). For flow induced vibration of flexible cylinders, surface vortices on the cylinders are caused not only by the mainstream velocity U, but also by the motion of the cylinders. In order to calculate the surface vortex strength of the vibrating cylinders, another term has to be added in Equation (2) to account for the motion of the cylinders. Therefore, if the mainstream direction is aligned with the x-direction (that is, $\alpha = 0$) the strength of the mth surface vortex element in one of the cylinders can be deduced as

$$\sum_{n=1}^{M} \gamma(s_n) K(s_n, s_m) \Delta s_n = \left[(-U + v_x) \frac{\mathrm{d}x_m}{\mathrm{d}s_m} \cos\alpha + v_y \frac{\mathrm{d}y_m}{\mathrm{d}s_m} \sin\alpha \right] + \sum_{i=1}^{I} \Delta\Gamma_i L(i,m) \tag{11}$$

where v_x and v_y are the vibration velocity of the cylinder in the x- and y-direction, respectively.

3. VALIDATION AGAINST A SINGLE RIGID CYLINDER

In order to verify the validity of the SVM, the flow past a rigid 2-D cylinder is calculated at $Re = 2.67 \times 10^4$ and compared with experimental measurements. The dimensionless time

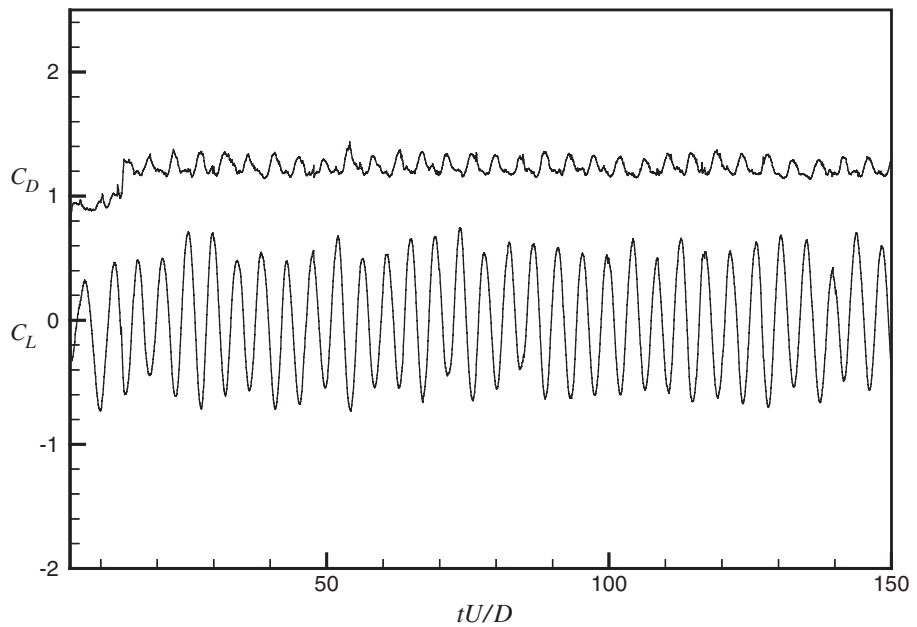

Figure 3. Time history of lift and drag coefficients of a rigid cylinder, $Re = 2.67 \times 10^4$.

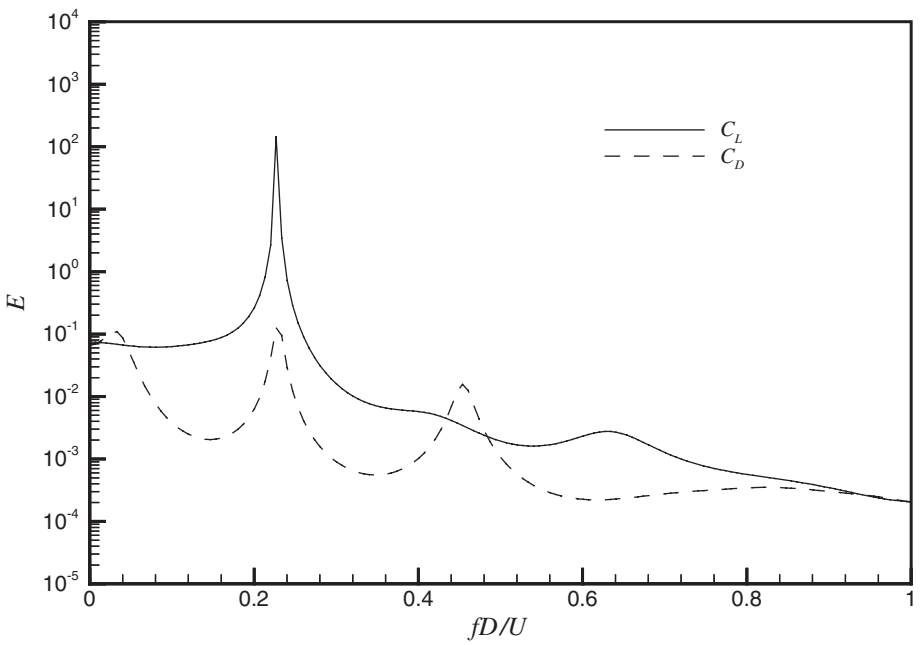

Figure 4. Spectral analysis of lift and drag force for a rigid cylinder, $Re = 2.67 \times 10^4$.

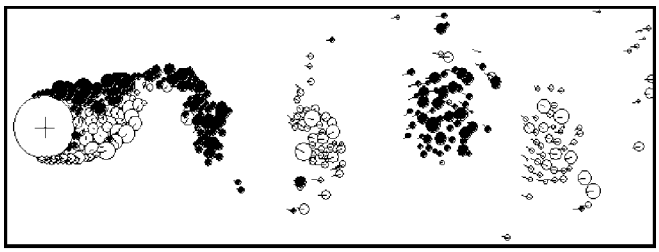

Figure 5. The vorticity map in the wake of a rigid cylinder at $Re = 2.67 \times 10^4$.

Table I. Comparison of the SVM calculated results with measurements for a rigid cylinder.

	Present calculation at $Re = 2.67 \times 10^4$	Measurement at $Re = 2.8 \times 10^4$ [26]
$\bar{C}_D$	1.229	1.18
C'_D	0.055	0.11
$\bar{C}_L$	0.005	—
C'_L	0.427	0.48
St^*	0.227	0.20

step in the computation is $\Delta tU/D = 0.075$. The time history of the lift and drag coefficient is shown in Figure 3, their auto-regressive moving average (ARMA) spectral analysis results in Figure 4, and the vorticity map at a particular time step is plotted in Figure 5. It is obvious that the lift force is nearly sinusoidal and its mean value is 0.005 (Table I), which can be considered essentially zero under the present numerical accuracy. The drag force is also periodic and its mean value is about 1.2. The drag force spectrum shows two significant frequencies, one is identical to the main frequency of the unsteady lift, i.e. the Strouhal frequency ($St^* = f_s D/U$, f_s is the shedding frequency), the other is double that of St^*, as expected. The vorticity map composes alternate negative and positive vortices, i.e. the Karman vortex street. It can be seen that the simulation results reflect the main features of the flow past a rigid 2-D cylinder. The calculated mean drag coefficient $\bar{C}_D$, rms lift coefficient C'_L, and St^* compared reasonably well with the measurements of West and Apelt [26] at $Re = 2.8 \times 10^4$ (Table I).

4. NUMERICAL RESULTS FOR A SINGLE FLEXIBLE CYLINDER

To validate the proposed vortex–cylinder interaction model, the flow induced vibration of a flexible cylinder at different reduced damping parameter and natural frequency is simulated by the SVM and the results are compared with experimental data.

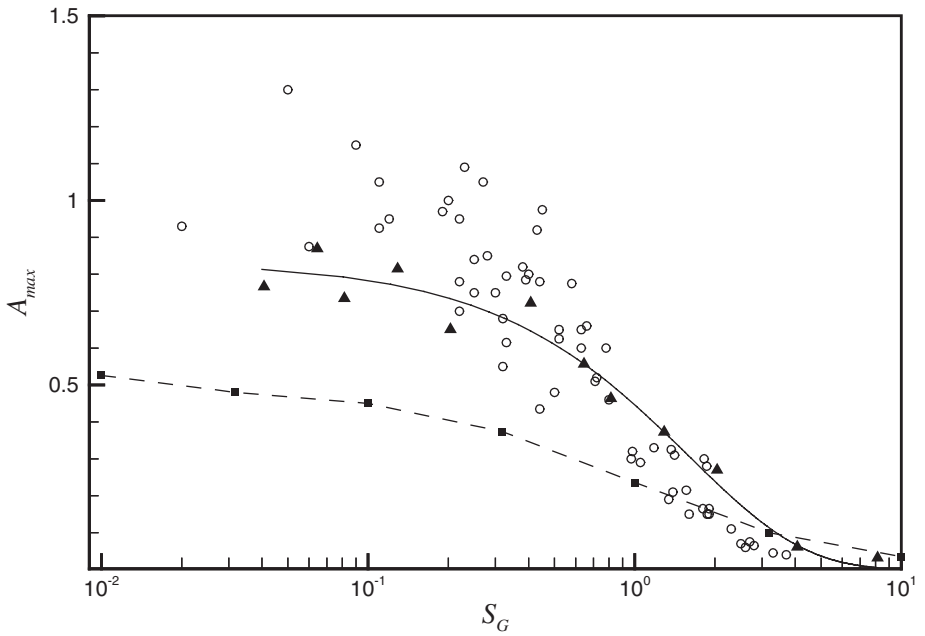

Figure 6. Flow-induced cross-flow maximum vibration amplitude versus S_G. ○: experimental data compiled by Skop and Balasubramanian [27]; ▲: present results for $Re = 2.67 \times 10^4$, $M = 10$; ■: computational results of Newman and Karniadakis [11] for $Re = 200$, $M = 10$.

4.1. Amplitude limiting vibration

One significant characteristics of flow-induced vibration of cylinders is that the vibration exhibits a self-limiting cycle. This means that the upper bound for the amplitude response approaches a limit, as the reduced damping parameter tends to zero. To verify the ability of the new vortex–cylinder interaction model, a single cylinder vibrating freely in a uniform flow is calculated at $Re = 2.67 \times 10^4$. The reduced damping parameter, $S_G = 8\pi^2 St^{*2} M\zeta_S$, varies from 0.04 to 8.14, and M is chosen to be 5 and 10.

A comparison of the experimental and computational results of the dimensionless maximum vibration amplitude A_{max} in the y-direction versus S_G is plotted in Figure 6. The open symbols represent the experimental data compiled by Skop and Balasubramanian [27]. The filled squared symbols and the dashed line are the computational results of Newman and Karniadakis [11]. The filled triangle symbols are the present results, which are scattered around a small tolerance zone, and the solid line is an exponential approximation of the calculated data. It can be seen that both results show an amplitude limiting response as S_G approaches zero, and at S_G less than about 0.1, the vibration amplitude does not have any increase. Compared to the results of Newman and Karniadakis [11], the present simulation results are consistent with experimental measurements, and the maximum vibration amplitude is as high as $0.88D$. The calculated maximum vibration amplitude is in good agreement with experimental results, especially in the high S_G (e.g. $S_G > 0.4$) range. The main reason for the slightly under-predicted

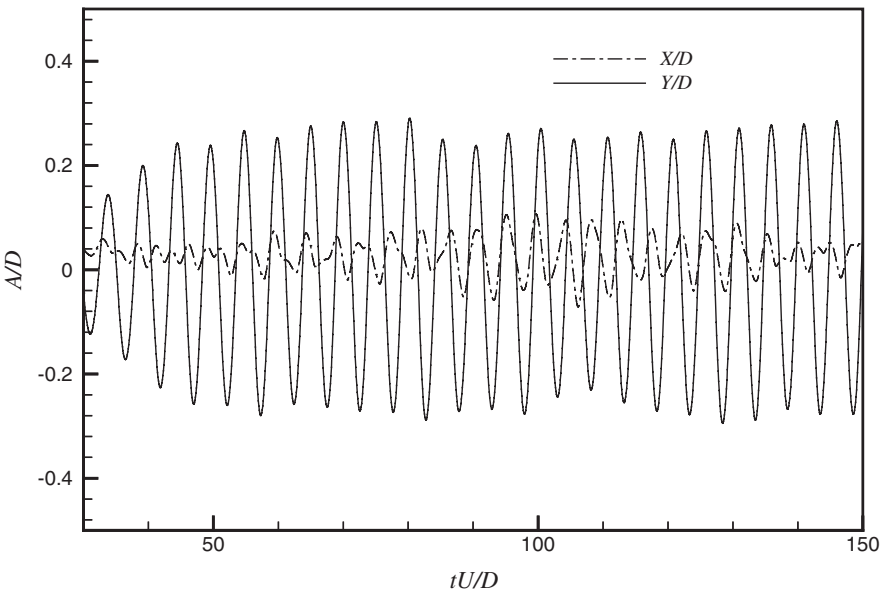

Figure 7. Time history of flow induced vibration of single flexible cylinder at $S_G = 1.29$.

A_{max} at low S_G might be due to the fact that the present computation is carried out at theoretical lock-in point ($f_N = f_0$, where f_N is the natural frequency of the flexible cylinder and f_0 is the shedding frequency of a rigid cylinder), while the maximum vibration amplitude occurs in the real lock-in point ($f_N = f_s$, f_s is the shedding frequency of the flexible cylinder and its value is not known *a priori*). Another reason could be due to difference in such parameters as M, and possible 3-D effects in the experiment. Nevertheless, the agreement between the present simulation and experimental data is satisfactory over a large range of S_G.

Figure 7 is the comparison of the normalized displacement in x- and y-direction for a flexible cylinder at $S_G = 1.29$. It can be seen that the displacement in the y-direction is much larger than that in the x-direction as expected. So in the following, the discussion is concentrated on the y-direction vibration.

The time histories of the normalized displacement Y/D for different S_G at lock-in ($f_N/f_0 = 1.0$) are plotted in Figure 8. These plots clearly show that Y/D increases with decreasing S_G. At $S_G = 8.14$, Y/D is very small (~ 0.04), and at $S_G = 1.29$, Y/D increases to 0.35. However, at $S_G = 0.129$, Y/D is about 0.8, which is close to the maximum Y/D of 0.88.

4.2. Non-linear flow induced vibration response

As a result of fluid–cylinder interaction, the flow induced vibration of a 2-D flexible cylinder is highly non-linear. To quantify this effect, the response of a 2-D flexible cylinder with different natural frequencies at $S_G = 1.29$ and $M = 10$ is calculated. The ratio of the flexible cylinder natural frequency to the rigid cylinder shedding frequency (f_N/f_0) is chosen to vary from 0.44 to 2.2. The dimensionless vibration frequency (f_s/f_0) and amplitude (A/D) of the cylinder in the y-direction are shown in Figures 9 and 10, respectively, while the dimensionless dominant

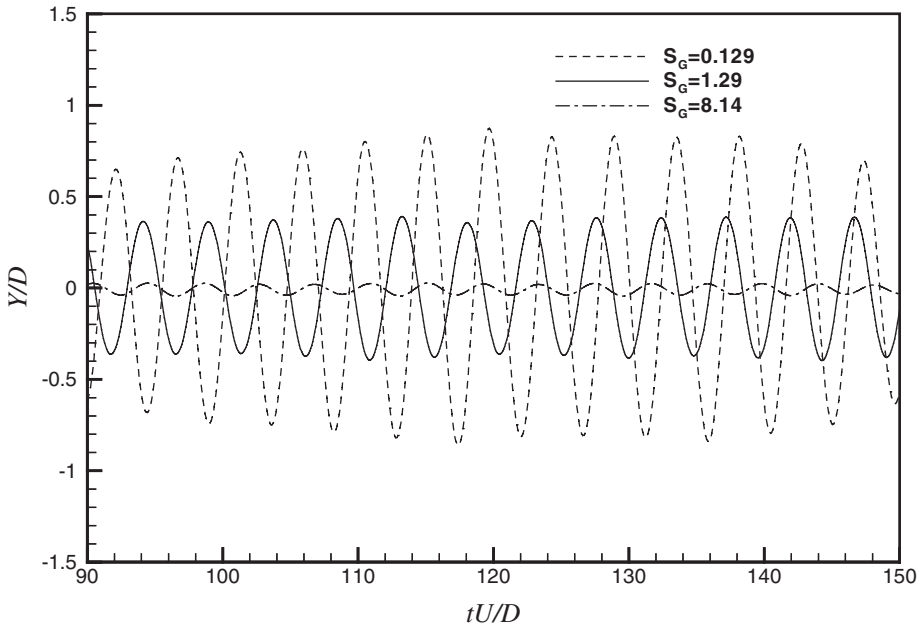

Figure 8. The time history of flow induced vibration of a flexible cylinder at different reduced damping parameters.

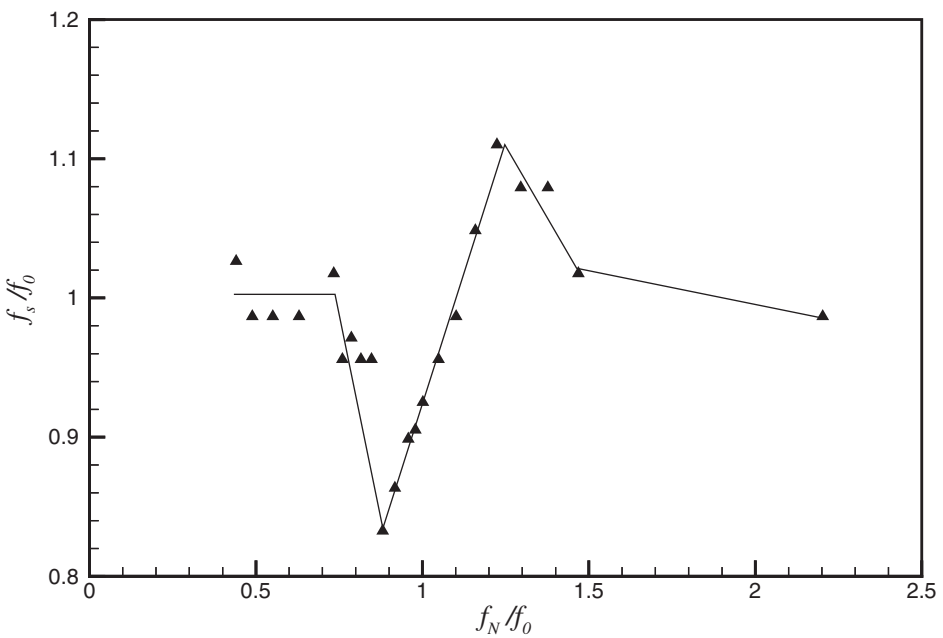

Figure 9. Flow-induced cross-flow vibration frequency versus natural frequency at $S_G = 1.29$ and $M = 10$.

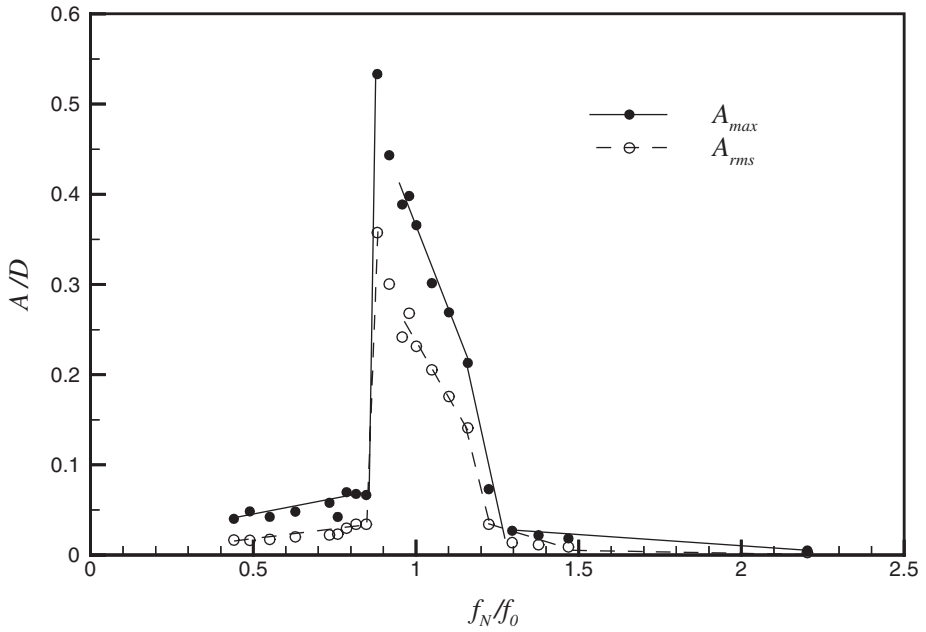

Figure 10. Flow-induced cross-flow vibration amplitude versus dimensionless natural frequency at $S_G = 1.29$ and $M = 10$. A_{max} is the maximal vibration amplitude in cross flow direction, while A_{rms} is the rms value of vibration amplitude in cross flow direction. (Symbols are the computational values, and lines are theirs segment approximation.)

frequency of the lift signal (f_L/f_0) and rms lift coefficient C'_L are shown in Figures 11 and 12, respectively. All quantities are plotted against the dimensionless natural frequency f_N/f_0. The lock-in region, where (f_s/f_0) and (f_L/f_0) vary linearly with the natural frequency of the cylinder, is clearly shown in Figures 9 and 11, and occurs at about $f_N/f_0 = 0.9$–1.2. Outside this region, the frequencies (f_s/f_0) and (f_L/f_0) gradually approach the shedding frequency of the rigid cylinder. From Figure 10, it can be seen that in the lock-in region the maximum value of the y-direction vibration amplitude is $A_{max} = 0.53$ and this does not occur at where the natural frequency is equal to the rigid cylinder shedding frequency, but at a position where the natural frequency is less than the rigid cylinder shedding frequency, i.e. at $f_N/f_0 = 0.9$. This is in agreement with the experimental result of Govardhan and Williamson [28] where they found that the maximum vibration amplitude occurs at $U_r St^* = f_0/f_N = 1.1$–1.2. The maximum lift coefficient is $C_{Lrms} = 2.00$ and occurs at $f_N/f_0 = 0.9$ (Figure 12), which is also the location of the maximum vibration amplitude.

In different regions, the coupling of fluid and structure has different influence. Figure 13 shows the time histories of Y/D in different regions, $f_N/f_0 = 0.50$ represents the pre-lock-in region, $f_N/f_0 = 1.0$ the lock-in region, and $f_N/f_0 = 1.49$ the post-lock-in region. It can be seen that in the lock-in region, Y/D is much larger, while in the pre- and post-lock-in region, Y/D in both cases is very small, and there is a phase difference between the three curves. The time histories of C_L in the pre- and post-lock-in regions are plotted in Figure 14. It can be

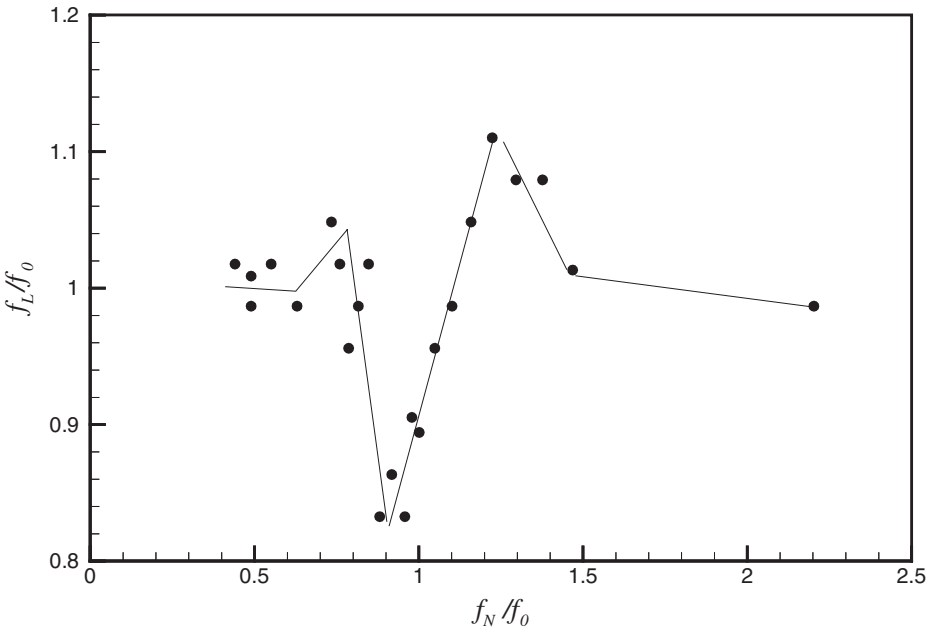

Figure 11. Lift frequency of vibration cylinder versus natural frequency at $S_G = 1.29$ and $M = 10$.

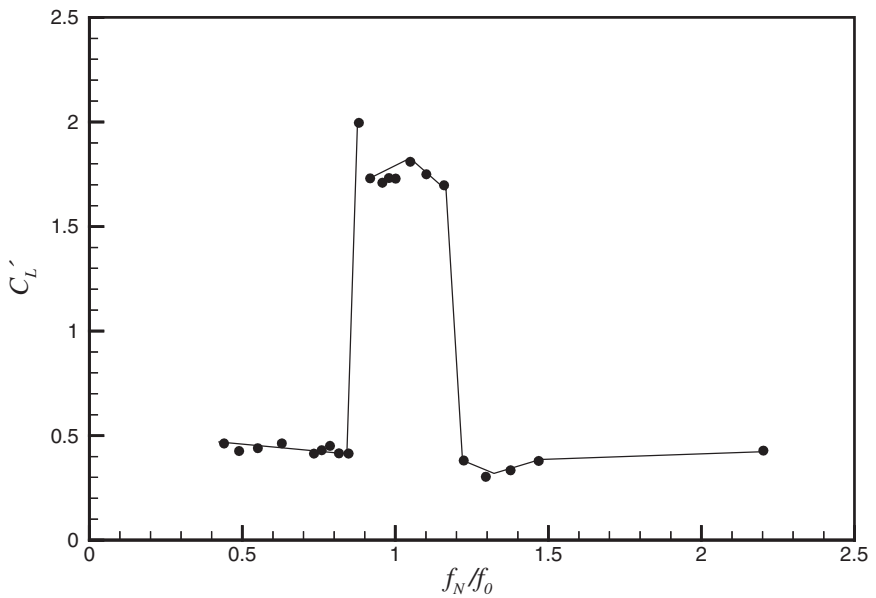

Figure 12. Lift coefficient of vibration cylinder versus natural frequency at $S_G = 1.29$ and $M = 10$.

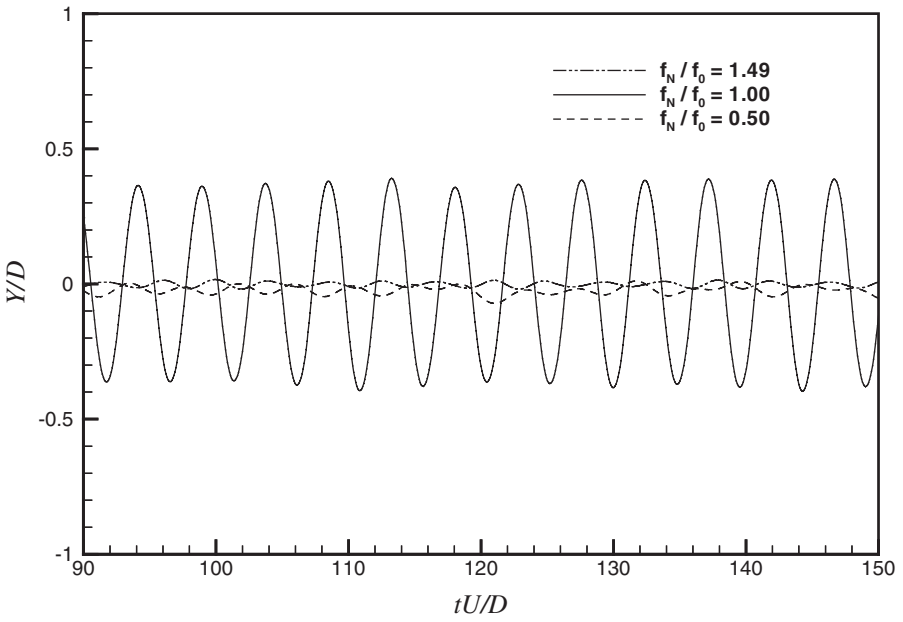

Figure 13. The time history of y-direction vibration responses of a flexible cylinder at different natural frequencies for $Re = 2.67 \times 10^4$, $S_G = 1.29$, and $M = 10$.

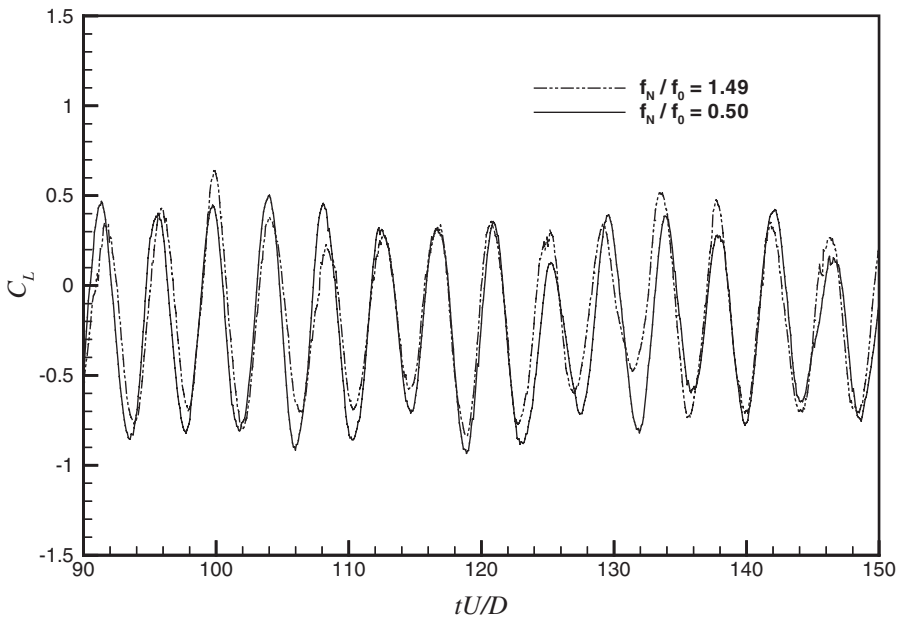

Figure 14. The time history of lift coefficient of a freely vibrating cylinder at different natural frequencies for $Re = 2.67 \times 10^4$, $S_G = 1.29$, and $M = 10$.

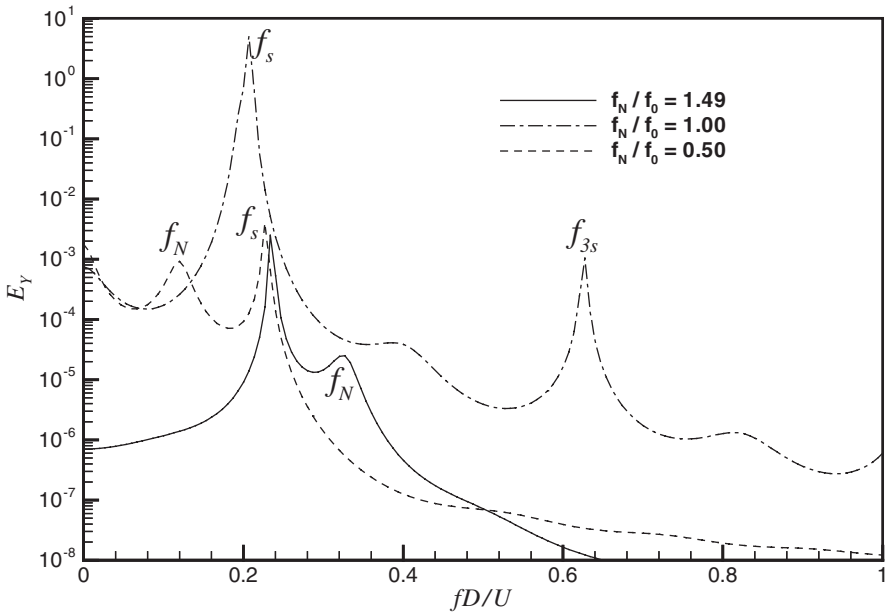

Figure 15. The frequency spectrum of y-direction vibration responses of a flexible cylinder at different natural frequencies for $Re = 2.67 \times 10^4$, $S_G = 1.29$, and $M = 10$.

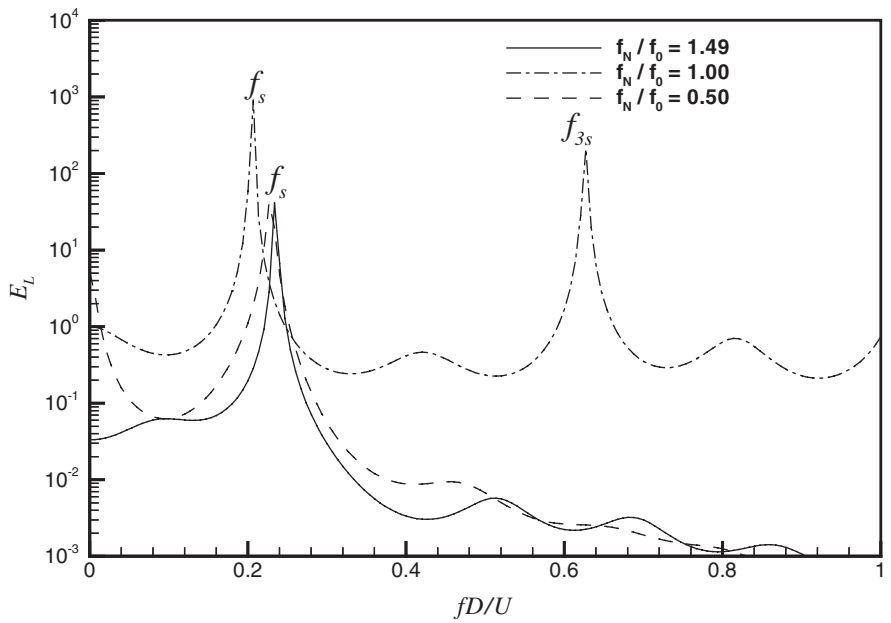

Figure 16. The frequency spectrum of lift coefficient of a freely vibrating cylinder at different natural frequencies for $Re = 2.67 \times 10^4$, $S_G = 1.29$, and $M = 10$.

Table II. Comparison of the SVM calculated dynamic characteristics of a freely vibration cylinder at different natural frequencies for $Re = 2.67 \times 10^4$, $S_G = 1.29$, and $M = 10$.

	$f_N/f_0 = 0.50$	$f_N/f_0 = 1.00$	$f_N/f_0 = 1.49$	$f_N/f_0 = 1.00^*$
C'_L	0.379	1.732	0.426	0.552
A_{rms}/D	0.009	0.268	0.016	0.105
f_N	0.111	0.205	0.330	0.206
f_s	0.224	0.205	0.231	0.206

*The results of this column are that neglect the influence of the cylinder velocity on surface vortices.

observed that the time series of these two C_L are nearly in-phase. Figures 15 and 16 show the frequency spectrum of Y/D and C_L in different regions, respectively. It can be seen that Y/D and C_L show the same major frequency, i.e. in the lock-in region they both exhibit f_s and its third harmonic, while in the pre-lock-in and post-lock-in region, only f_s is evident. In the lock-in region, f_s coincide with f_N of the cylinder. Outside the lock-in region, both f_s, and f_N are clearly visible from the spectral plots.

The flow induced vibration of a flexible cylinder at $S_G = 1.29$ in lock-in region ($f_N/f_0 = 1.0$) was also simulated, on the action of the structure on the flow field is only regarded as the results of free vortices moving with the cylinder and the influence of cylinder velocity to surface vortices is neglected. It is denoted as the 'velocity-ignoring model' when compared with the proposed model. The calculated C'_L, A_{rms}/D, f_N, and f_s of the 'velocity ignoring model' are shown in Table II together with the adopted model of the freely vibrating cylinder at $S_G = 1.29$ in different regions. The rms vibrating amplitude of the 'velocity ignoring model' in the lock-in region is much smaller than the experimental results [27]. The fluctuation lift of the 'velocity-ignoring model' is so small that just a little bigger than that of a fixed cylinder. This indicates that in order to calculate the flow-induced vibration of cylinders by the SVM the influence of cylinder velocity to surface vortices has to be included in the model. In the present model, in the lock-in region, the calculated C'_L is about four times that of the stationary rigid cylinder, and in the pre-lock-in and post-lock-in region, it is nearly the same as that of the rigid cylinder, while A_{rms}/D in the lock-in region is about 17 times that in the pre-lock-in region and 29 times that in post-lock-in region. This shows that fluid–cylinder interaction is much more prominent in the lock-in region than in the pre-lock-in and post-lock-in regions. The shedding frequency of the fluid–cylinder system in different regions is close to that of the rigid cylinder, thus implying that the induced force and the resulting vibration are fundamentally controlled by the Strouhal periodicity.

4.3. Vorticity map

Finally, the near wake of the cylinder with different vibration amplitude is examined. Figure 17 gives the vorticity map of the freely vibrating cylinder at the crest of its vibration cycle in the lock-in region ($f_N/f_0 = 1.0$) for different reduced damping parameters. The position of the original center of the cylinder (represented by a cross) is indicated for reference. Compared with the rigid cylinder (Figure 5), the wake width of the vibrating cylinder is much wider. It is obvious that with increasing vibration amplitude, the wake width of the vibrating cylinder also increases. The vorticity map of the cylinder with a smaller vibration amplitude ($A_{max} = 0.35D$,

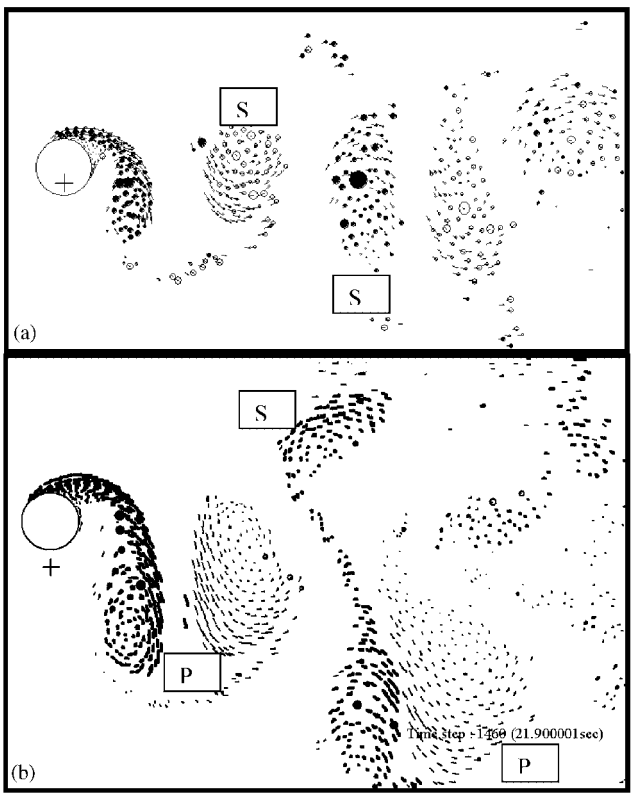

Figure 17. Vorticity maps of the freely vibration cylinders at the uppermost point in its motion cycle. (a) $S_G = 1.29$, 2S mode; (b) $S_G = 0.129$, P+S mode.

$S_G = 1.29$) shows a 2S mode (Figure 17(a)), i.e. two single vortices formed per cycle, while the vorticity map of the larger vibration cylinder ($A_{max} = 0.80D$, $S_G = 0.129$) indicates a P+S mode (Figure 17(b)), i.e. a pair of vortices and a single vortex formed per cycle. This means that with small vibration amplitude, the near wake of the cylinder approximates to a stable Karman vortex street, while with large vibration amplitude the near wake of the cylinder shows a transient P+S mode behaviour.

5. FLOW INDUCED VIBRATION OF TWO CYLINDERS

Having demonstrated the ability of the vortex–cylinder interaction model to simulate a single flexible cylinder in a cross-flow, the new model is then applied to calculate the flow induced vibration of two tandem cylinders and two side-by-side cylinders. It is a well-known fact that two stationary cylinders can produce many different flow interference patterns such as shielding flow pattern and bistable flow pattern depending on the spacing ratio and configuration. When the two cylinders are allowed to vibrate freely, the flow patterns and the fluid–cylinder

Table III. Comparison of the SVM calculated results with measurements for two rigid cylinders in tandem configuration.

	$L/D = 2.0$		$L/D = 1.5$	
	Alam *et al.* [29] $Re = 6.5 \times 10^4$	Present calculation	Alam *et al.* [29] $Re = 6.5 \times 10^4$	Present calculation
$\bar{C}_D$ (upstream)	1.05	0.866	1.10	1.161
$\bar{C}_D$ (downstream)	−0.25	−0.411	−0.40	−0.559
C_D (upstream)	0.024	0.036	0.024	0.027
C'_D (downstream)	0.130	0.072	0.147	0.121
$\bar{C}_L$ (upstream)	—	−0.025	—	−0.122
$\bar{C}_L$ (downstream)	—	−0.044	—	0.071
C'_L (upstream)	0.11	0.126	0.28	0.181
C'_L (downstream)	0.64	0.182	0.48	0.252
St^*	0.139	0.144	0.140	0.142

interactions could be even more complicated. The present simulations on tandem and side-by-side arrangements are performed at spacing ratios $L/D = 1.5$ and $L/D = 2.0$, $S_G = 1.29$ and $S_G = 0.645$, mass ratio $M = 10$, $Re = 2.67 \times 10^4$, and $f_N/f_0 = 1.0$.

5.1. Tandem arrangement

The present prediction of force coefficients and Strouhal frequencies St^* for two rigid cylinders in tandem at spacing ratios of 2.0 and 1.5 are compared with the experimental measurements of Alam *et al.* [29] in Table III. Good agreement between calculation and experiment is obtained except for the fluctuation lift of the down stream cylinder, which is less than the experimental results. The reason for this error may be that when calculating the pressure of the downstream cylinder only the effect of separation was considered, but not the effect of reattachment of the upstream cylinder vortices in the calculation Equation (4).

Table IV gives the simulation results of the force coefficients and the Strouhal frequencies of two freely vibrating cylinders in tandem at different spacing ratios and reduced damping parameters. The mean drag coefficient of the downstream cylinder is negative or approaching zero for all cases examined, thus indicating that the two flexible cylinders still exhibit the characteristics of a shielded flow. The mean drag coefficients of the two flexible cylinders vary differently with S_G. For $S_G = 1.29$, the drag coefficients of the upstream and downstream cylinder are both larger than the corresponding rigid case, while for $S_G = 0.645$, the drag coefficients of the downstream cylinder approaches zero, and the drag coefficient of the upstream cylinder is approximately 1.0. It seems that at $S_G = 1.29$, the effect of flow induced vibration on the two cylinders is similar to that on a single cylinder, i.e. to increase the drag force, but at $S_G = 0.645$, the effect of cylinder vibration on the two flexible cylinders is to cause them to act more like two rigid cylinders arranged in a larger spacing ratio.

Compared with rigid cylinders the fluctuating forces induced on flexible cylinders are all increased. As the spacing ratio decreases from 2.0 to 1.5, the fluctuating forces of the upstream and downstream cylinder increase dramatically for $S_G = 1.29$, while the fluctuating forces only vary a little for the case where $S_G = 0.645$. This means that at $S_G = 0.645$, the effect of spacing

Table IV. Force coefficients and shedding frequency of two flexible cylinders in tandem configuration.

	$L/D = 2.0$		$L/D = 1.5$	
	$S_G = 1.29$	$S_G = 0.645$	$S_G = 1.29$	$S_G = 0.645$
$\bar{C}_D$ (upstream)	1.355	1.065	1.265	0.984
$\bar{C}_D$ (downstream)	−0.350	−0.080	−0.231	0.010
C'_D (upstream)	0.204	0.459	0.403	0.493
C'_D (downstream)	0.155	0.630	0.296	0.530
$\bar{C}_L$ (upstream)	−0.158	−0.140	−0.011	−0.013
$\bar{C}_L$ (downstream)	−0.057	−0.016	0.028	0.009
C'_L (upstream)	0.435	0.969	0.927	0.961
C'_L (downstream)	0.283	0.552	0.374	0.487
St^* (upstream)	0.198	0.165	0.192	0.177
St^* (downstream)	0.198	0.165	0.192	0.162

ratio on the fluctuating forces is small compared with the case where $S_G = 1.29$, and it seems that, at $S_G = 0.645$, S_G is the prominent parameter that affects the lift force for these two spacing ratios. Possible explanation for this behaviour could be due to the enhancement of vortex shedding from the upstream cylinder as a result of the vibration of the two cylinders. This enhancement increases the mean force of the upstream cylinder, and at the same time increases the fluctuating forces of the two cylinders. As for the downstream cylinder, which has a steady stream of vortices impinging on it, a change of vortex shedding pattern only affects the fluctuating forces and not the mean forces.

From Table IV, it is shown that the shedding frequency of flexible cylinders is dominated by the damping ratio parameter S_G rather than the spacing ratio. For $S_G = 1.29$, the Strouhal frequencies St^* is about 0.19, while for $S_G = 0.645$, it is about 0.17. They are all larger than the Strouhal frequencies of the fixed cylinders (in Table III).

The time histories of the X/D and Y/D displacements of two cylinders in tandem at $L/D = 1.5$ and $S_G = 1.29$ and 0.645 are shown in Figure 18. It is clear that the vibration amplitude in the y-direction is much larger than that in the x-direction. Furthermore, the vibration amplitude of the upstream cylinder in the y-direction is larger than that of the downstream cylinder, which agrees with the experimental results of Jendrzejczyk's [30] at small spacing. The vibration amplitude of the cylinders appears to be dependent on S_G. The vibration amplitude of the upstream cylinder increases as S_G decreases, while the opposite is true for the downstream cylinder. The upstream cylinder develops the dominant vibration and disrupts the vortex shedding of the downstream cylinder, so the maximum vibration amplitude occurs in the upstream cylinder. Of course, the vibration amplitudes of the two cylinders are much smaller than that of a single cylinder due to proximity interference and wake interference.

5.2. *Side-by-side arrangement*

Table V compares the SVM calculated results with the measurements of Bearman and Wadcock [31] for two side-by-side rigid cylinders at spacing ratios 2.0 and 1.5. The multi-frequency behavior occurs at $L/D = 1.5$ in the simulation results as expected. It can be seen

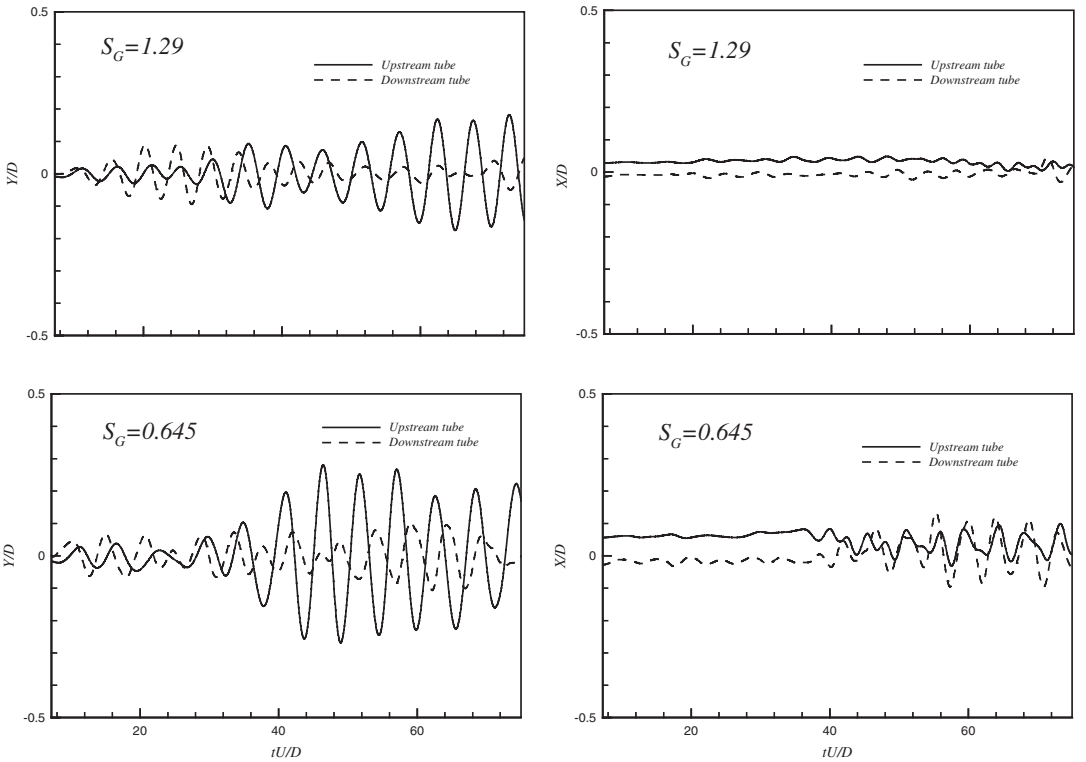

Figure 18. Time history of flow induced vibration of two cylinders in tandem ($L/D = 1.5$) at different reduced damping parameters.

Table V. Comparison of the SVM calculated results with measurements for two rigid cylinders in side-by-side configuration.

	$L/D = 2.0$		$L/D = 1.5$	
	Bearman and Wadcock [31] $Re = 2.5 \times 10^4$	Present calculation	Bearman and Wadcock [31] $Re = 2.5 \times 10^4$	Present calculation
$\bar{C}_D$	1.40	1.313	1.29	1.885
C'_L	0.22	0.417	0.34	0.320
			0.11	0.136
St^*	0.21	0.224	0.21	0.234
			0.34	0.288

that the calculated force coefficients and Strouhal frequency are in good agreement with measured data. The only exception is the over-prediction of the drag coefficient at $L/D = 1.5$.

For two side-by-side cylinders, compared with their rigid counterpart, the mean force coefficients of the flexible cylinders only decrease slightly (Table VI), while the fluctuating force

Table VI. Force coefficients and shedding frequency of two flexible cylinders in side-by-side configuration.

	$L/D = 2.0$		$L/D = 1.5$
	$S_G = 1.29$	$S_G = 0.645$	$S_G = 1.29$
$\bar{C}_D$ (upper)	1.322	1.070	1.796
$\bar{C}_D$ (lower)	1.227	0.935	1.657
C'_D (upper)	0.916	1.073	0.884
C'_D (lower)	0.823	0.923	0.821
$\bar{C}_L$ (upper)	0.256	0.152	0.111
$\bar{C}_L$ (lower)	−0.046	0.244	−0.166
C'_L (upper)	1.109	1.163	0.854
C'_L (lower)	1.171	0.780	0.672
St^* (upper)	0.196	0.196	0.192 0.385
St^* (lower)	0.196	0.196	0.192 0.385

coefficients increase significantly. From Table VI, it is obvious that the well-known double-frequency (corresponding to bi-stable phenomenon) also occurs for two flexible cylinders at the spacing ratio 1.5 in the lock-in region where the shedding frequencies of the two cylinders is locked into the natural frequency of the coupled system.

The time histories of the flow induced vibration of the two side-by-side flexible cylinders at $L/D = 2.0$ and $S_G = 1.29$ and 0.645 are shown in Figure 19. At $S_G = 1.29$, Y/D is larger than X/D. However, compared with a single flexible cylinder, the difference between Y/D and X/D amplitude is no longer so significant (Figure 7). At $S_G = 0.645$, the amplitude of Y/D for the upper cylinder is still larger than that of X/D, but the opposite is true for the lower cylinder. This indicates that with an increase in S_G, the x- and y-direction coupling between the two vibrating cylinders in a side-by-side arrangement has increased. The vibration responses of the upper and lower cylinder at $S_G = 1.29$ and 0.645 are nearly anti-phase in the y-direction and in-phase in the x-direction. This indicates that, at $L/D = 2.0$, the vortices shed from the two flexible cylinders are still symmetrical, and no jetstream is formed between the cylinders.

From the numerical results of flow-induced vibration of two tandem and side-by-side cylinders, it can be seen that the fluctuating force coefficients of the coupled system are increased compared with their rigid counterparts. For tandem arrangement, the vibration amplitudes of the two flexible cylinders are small due to proximity and wake interference. As for side-by-side arrangement, increasing the reduced damping parameter, the x- and y- direction coupling between the two vibrating cylinders is increased, and the vibration amplitude in the y-direction is not always larger than that in the x-direction.

Finally some ideas on the free vortex numbers and the computational times used in the present computation are given. For a single stationary cylinder, the maximum free vortex number is about 700, while for a single cylinder with large vibration amplitude, the maximum free vortex number is up to 3000. With an increase in free vortex the computational time is also increased. The computational time for 2000 time steps in a Pentium III PC can range

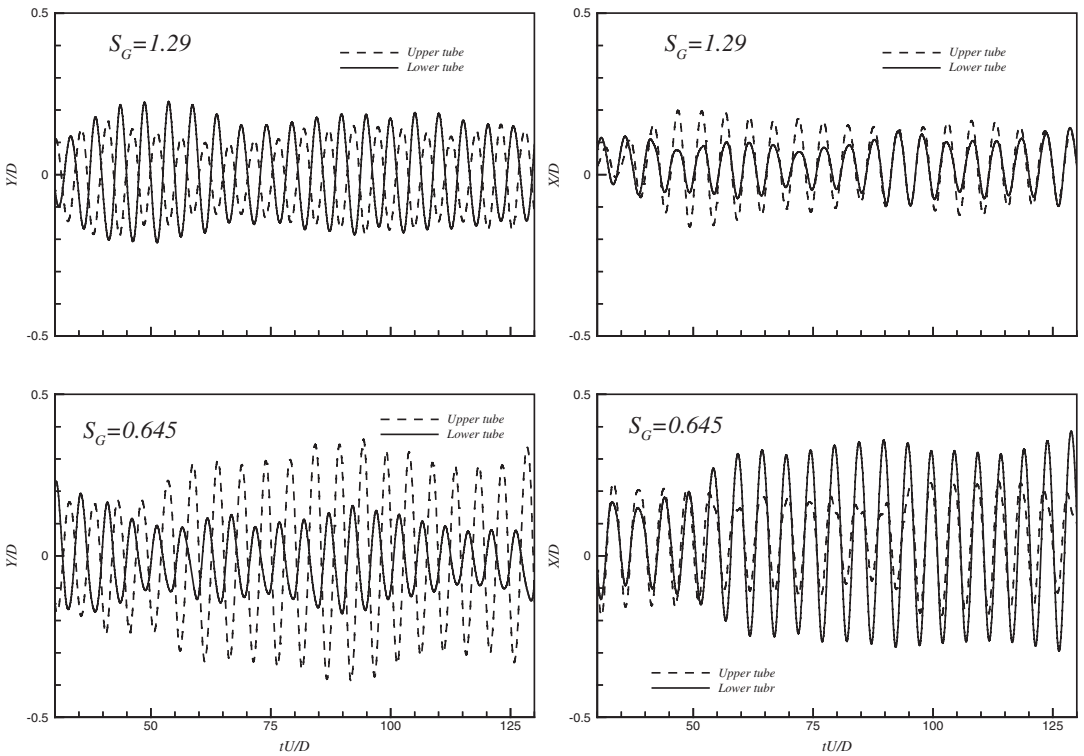

Figure 19. Time history of flow induced vibration of two side-by-side cylinders ($L/D = 2.0$) at different reduced damping parameters.

from about 4 h for a single fixed cylinder to about 12 h for two freely vibrating cylinders. Therefore the approach is more time saving as compared to the mesh-based method.

6. CONCLUSIONS

In order to simulate the flow induced vibration of heat exchanger tube bundles a new grid-free vortex cylinder interaction model based on SVM is proposed. The vibrations of flexible cylinders are simulated with this model at a sub-critical Reynolds number $Re = 2.67 \times 10^4$, and the response of the cylinder, the induced unsteady forces, the vibration frequency and the vorticity map are all examined. The calculated results are compared with other experimental and computational data.

The numerical simulation replicates the amplitude limiting phenomenon and the non-linear characteristics of a freely vibrating 2-D cylinder. The maximum vibration amplitude is in good agreement with experimental data. The lock-in phenomenon is clearly evident and the maximum vibration amplitude point is determined to locate at $f_N/f_0 = 0.9$, which also agrees with experimental result. The amplitude of vibration can be as high as $0.88D$ for the case

investigated. As vibration amplitude increases, the lift force amplitude also increases. With an increase in the vibration amplitude, the vortex pattern in the near wake changes significantly.

The present method is also successfully applied to simulate flow induced vibration of two cylinders arranged in tandem for large amplitude vibration and side-by-side in lock-in region at different spacing and reduced damping parameters. The force coefficients, shedding frequencies and vibration time histories of the coupled fluid–structure system are all investigated. The results show that flow induced vibration has significant influence on the dynamic response of the cylinders. Hence, the new model developed is general enough to account for the fluid–structure interaction in multi-cylinder problems. Therefore, the present method provides a viable technique to simulate complex flow induced vibration problems found in heat exchanger tube bundles at sub-critical Reynolds number.

ACKNOWLEDGEMENTS

The authors wish to thank the Research Grants Council of the Hong Kong Special Administrative Region, China, for its support through Grant No. PolyU 5163/01E.

REFERENCES

1. Weaver DS, Fitzpatrick JA. A review of cross flow induced vibrations in heat exchanger tube arrays. *Journal of Fluids and Structures* 1988; **2**:73–93.
2. Ziada S, Oengoren A. Vortex shedding and acoustic resonance in an in-line tube bundle. Part I: vorticity shedding. *Journal of Fluids and Structures* 1992; **6**:271–292.
3. Zdravkovich MM. On suppressing matastable interstitial flow behind a tube array. *Journal of Fluids and Structures* 1993; **7**:245–252.
4. Polar DR, Weaver DS. Vortex shedding in normal triangular tube arrays. *Journal of Fluids and Structures* 1995; **9**:1–17.
5. Austermann R. Stability behaviour of a single flexible cylinder in rigid tube arrays of different geometry subjected to cross-flow. *Journal of Fluids and Structures* 1995; **9**:303–322.
6. Romberg O, Popp K. The influence of upstream turbulence on the stability boundaries of a flexible tube in a bundle. *Journal of Fluids and Structures* 1998; **12**:153–169.
7. Chen SS, Srikantiah GS. Motion-dependent fluid force coefficients for tube arrays in crossflow. *Journal of Pressure Vessel Technology* 2001; **123**:429–436.
8. Price SJ. A review of theoretical models for fluidelastic instability of cylinder arrays in cross-flow. *Journal of Fluids and Structures* 1995; **9**:463–518.
9. Belvins RD. *Flow Induced Vibrations* (2nd edn). Krieger: Florida, 1994.
10. Ichioka T, Kawata Y, Nakamura T, Izumi H, Nakamura T, Fujita K. Two-dimensional flow analysis of fluid cylinder interaction around a cylinder and a row of cylinders. In *Proceedings of the ASME Symposium on Flow-Induced Vibrations*, PVP-vol. 273. 1994; 33–41.
11. Newman DJ, Karniadakis GE. A direct numerical simulation study of flow past a freely vibration cable. *Journal of Fluid Mechanics* 1997; **334**:95–136.
12. So RMC, Liu Y, Chan ST, Lam K. Numerical studies of a freely vibration cylinder in across-flow. *Journal of Fluids and Structures* 2001; **15**:845–866.
13. Ichioka T, Kawata Y, Nakamura T, Izumi H, Kobayashi T, Takamatsu H. Research on fluid elastic vibration of cylinder arrays by computational fluid dynamics (analysis of two cylinders and a cylinder row). *JSME International Journal*, *Series B*: *Fluid and Thermal Engineering* 1997; **40**(1):16–24.
14. Kassera V, Strohmeier K. Simulation of tube bundle vibrations induced by cross-flow. *Journal of Fluids and Structures* 1997; **11**:909–928.
15. Schroder K, Gelbe H. Two- and three-dimensional CFD-simulation of flow-induced vibration excitation in tube bundles. *Chemical Engineering and Processing* 1999; **38**:621–629.
16. Liu Y, So RMC, Lau YL, Zhou Y. Numerical studies of two side-by-side elastic cylinders in a cross-flow. *Journal of Fluids and Structures* 2001; **15**:1009–1030.
17. Mittal S, Kumar V. Flow-induced oscillations of two cylinders in tandem and staggered arrangements. *Journal of Fluids and Structures* 2001; **15**:717–736.
18. Slaouti A, Stansby PK. Forced oscillation and dynamics response of a cylinder in a current investigated by the vortex method. In *Proceedings BOSS'94 Conference MIT*, 1994; 645–654.

19. Zhou CY, So RMC, Lam K. Vortex-induced vibrations of an elastic circular cylinder. *Journal of Fluids and Structures* 1999; **13**:165–189.
20. Lam K, Chan YF. A refined surface vorticity modelling of separated flow around a circular cylinder. In *Proceedings of the 1998 ASME Fluid Engineering Division Summer Meeting*, ASME: Washington, FED-vol. 245. 1998; 21–23.
21. Lam K, So RMC, Li JY. Flow around four cylinders in a square configuration using surface vorticity method. In *The Second International Conference on Vortex Methods*, Turkey, 2001; 115–122.
22. Lewis RI. *Vortex Element Methods for Fluid Dynamic Analysis of Engineering System*. Cambridge University Press: Cambridge, 1991.
23. Ogami Y, Akamatsu T. Viscous flow simulation using the discrete vortex method—the diffusion velocity method. *Computers and Fluids* 1991; **9**:433–441.
24. Zdravkovich MM. *Flow Around Circle Cylinders*. Oxford University Press: Oxford, 1997–2003.
25. Lewis RI. Surface vorticity modelling of separated flows from two-dimensional bluff bodies of arbitrary shape. *Journal of Mechanical Engineering Science* 1981; **23**:1–12.
26. West GS, Apelt CJ. Measurements of fluctuation pressures and forces on a circular cylinder in the Reynolds number range 10^4 to 2.5×10^5. *Journal of Fluids and Structures* 1993; **7**:227–244.
27. Skop RA, Balasubramanian S. A new twist on an old model for vortex-excited vibrations. *Journal of Fluids and Structures* 1997; **11**:395–412.
28. Govardhan R, Williamson CHK. Mean and fluctuating velocity fields in the wake of a freely-vibrating cylinder. *Journal of Fluids and Structures* 2001; **15**:489–501.
29. Alam MM, Moriya M, Takai K, Sakamoto H. Fluctuating fluid forces acting on two circular cylinders in a tandem arrangement at a subcritical Reynolds number. *Journal of Wind Engineering and Industrial Aerodynamics* 2003; **91**:139–154.
30. Jendrzejczyk JA, Chen SS, Wambsganss MW. Dynamic response of a pair of circular cylinders subjected to liquid cross flow. *Journal of Sound and Vibration* 1979; **67**:263–273.
31. Bearman PW, Wadcock AJ. The interaction between a pair of circular cylinders normal to a stream. *Journal of Fluid Mechanics* 1973; **61**:499–511.

